Turbulent flame propagation limits of polymethylmethacrylate particle cloud–ammonia–air co-combustion

Yu Xia [a, b], Nozomu Hashimoto [a*], Osamu Fujita [a]

[a] *Division of Mechanical and Space Engineering, Hokkaido University, Kita13 Nishi8, Kita-ku, Sapporo 060-8628, Japan*
[b] *Institute of Fluid Science, Tohoku University, 2-1-1 Katahira, Aoba-Ku, Sendai, Miyagi, 980-8577, Japan*

Abstract

Ammonia is a highly promising energy carrier for achieving a carbon-neutral society. The co-combustion of solid particle clouds–ammonia, in particular, is considered an efficient and feasible method of reducing carbon dioxide emissions. Understanding turbulent flame stabilization and extinguishment processes during the two-phase hybrid-mixture co-combustion of solid particle clouds–ammonia is essential for the co-combustion technology to be used in combustors. To the best of our knowledge, this is the first study to describe the turbulent flame propagation limits and associated mechanism on the co-combustion of solid particle clouds–ammonia–air. Turbulent flame propagation experiments on silica particle clouds–ammonia–air mixing combustion and polymethylmethacrylate (PMMA) particle cloud–ammonia–air co-combustion were conducted in this work using a novel fan-stirred constant-volume vessel to clarify the turbulent flame propagation limits and associate mechanism of solid particle cloud–ammonia–air co-combustion. Results showed that adding inert silica particles contracted the turbulent flame propagation limits of premixed ammonia–air mixtures. However, adding PMMA particles expanded and then contracted the turbulent flame propagation limits of a premixed ammonia–air mixture as the ammonia equivalence ratio increased from lean to rich. In the solid particle cloud–ammonia–air co-combustion, reactive particles induce two types of effects on the turbulent flame propagation limits of premixed ammonia–air mixtures: The local equivalence ratio increment effect is caused by adding volatile matter from preheated particles in the preheat zone of the flame front, and the heat sink negative effect is induced by the unburned particles.

Keywords: Turbulent flame propagation limit; Solid particle cloud combustion; Ammonia combustion; Co-combustion; Inert particle effect;

*Corresponding author. Tel.: +81-11-706-6386. E-mail address: nozomu.hashimoto@eng.hokudai.ac.jp

1. Introduction

Ammonia is generating a considerable interest in the combustion field as a possible alternative fuel for energy generation and transportation systems owing to its carbon-free property. Ammonia combustion produces no CO_2, SO_x, or soot. Furthermore, ammonia is easier to store and transport than hydrogen [1]. Recently, a novel method for producing ammonia as a renewable fuel was proposed [2]. Coal-fired power generation accounts for approximately 30% of the world's primary energy [3]. Although it is doubtful that other fuels will completely replace coal, the co-combustion of ammonia and pulverized coal in thermal power plants is a practical method of reducing CO_2 emissions. CO_2 and NO_x emissions from coal-fired boilers can be reduced through the co-combustion of pulverized coal–ammonia–oxidizer [3,4]. Therefore, the pulverized coal–ammonia–oxidizer co-combustion has immense potential and is one of the most promising pathways to a carbon-neutral society. Additionally, the method of the co-combustion of solid particle cloud and ammonia can also enable power generation from other solid particle clouds, such as solid waste and biomass fuel.

Stabilization and extinction of flame is a significant challenge for propulsion and energy systems [5]. Advances in our understanding of flame stability and extinguishment have resulted in the development of novel solutions for turbulent combustion systems [5]. Owing to the weak combustion intensity and ease with which they are extinguished of premixed ammonia–air flames, many studies have been conducted to clarify the extinction and stabilization characteristics of premixed ammonia flames. Hayakawa et al. [6] demonstrated the stabilization performance of premixed ammonia–air flames in a swirl combustor in the absence of any additives to enhance ammonia combustion. Colson et al. [7,8] described the non-premixed ammonia–methane jet flame stabilization regimes. Khateeb et al.[9] studied the stability limits of premixed swirl ammonia-air flames enriched with methane or hydrogen. Okafor et al. [10] demonstrated the flame stability of liquid ammonia spray via co-combustion ammonia spray and methane. Wiseman [11] studied the blow-out behavior of turbulent premixed ammonia–hydrogen flames. Xia et al. [1] and Lhuillier et al. [12] studied the turbulent burning characteristics of ammonia flame. Ichimura et al. and Hashimoto et al. [13,14] reported the turbulent flame propagation limits of ammonia–air and ammonia–methane–air premixtures and suggested that diffusional–thermal instability plays an important role in the extinction of ammonia flames during turbulent flame propagation. Although the co-combustion of solid particle clouds and ammonia is a promising solution to decrease the CO_2 emissions and move toward a carbon-free society, the fundamental turbulent flame extinction characteristics remain unknown to date.

Turbulent flame propagation velocity is one of the most essential physical properties for determining the performance of fuel combustion in combustors in terms of flame stability [15,16]. In our previous studies involving solid particle cloud–ammonia–diluted-oxidizer (diluted-oxidizer: 40% oxygen and 60% nitrogen) co-combustion [17,18], we discovered that the turbulent flame propagation velocity in solid particle cloud–ammonia co-combustion was higher than that of pure solid particle cloud combustion, and whether the turbulent flame propagation velocity of the co-combustion is higher than that of pure ammonia combustion is dependent on the equivalence ratio of the ammonia–oxidizer mixture. Therefore, we proposed and validated a mechanism comprising two effects to account for this phenomenon—the negative effect of unburned particles as a heat sink, and the local equivalence ratio increment effect by adding volatile matter released from the particles in the flame front's preheat zone [17,18]. Furthermore, it was suggested that the heterogeneous burning of char particles has a negligible effect on the turbulent flame propagation associated with co-combustion because of its slow combustion process [18]. Additionally, for high-fuel-ratio coals, the co-combustion of pulverized coal and ammonia can enhance flame stability [19]. Although this co-combustion turbulent flame propagation mechanism is applicable to the stabilized flame propagation phenomenon, the fundamental turbulent flame extinction mechanism of co-combustion of a solid particle cloud–ammonia–air two-phase hybrid mixture has not been reported to date.

Therefore, we aimed to clarify the fundamental turbulent flame propagation limitations and extinction mechanism of solid particle cloud–ammonia–air co-combustion in a near homogeneous turbulent flow field. To achieve this aim, the polymethylmethacrylate (PMMA) solid particles were used in co-combustion experiments as i) PMMA particles can be treated as the representative particle of volatile particle because, after being preheated, they can be "cleanly" devolatilized to its monomer, MMA; ii) PMMA particles can be easily made as quasi-monodispersed to minimize the inter-particle interaction effect [20]; iii) the important finding from present research should be common in solid particle cloud–gaseous fuel co-combustion for various volatile solid fuels, such as coal and biomass fuels. Furthermore, to separately examine the thermal heat sink effect induced by the particles in solid particle cloud–ammonia co-combustion, the experiments on silica particle cloud–ammonia mixing combustion were also conducted.

Experimental results may contribute to the application of solid particle cloud–ammonia co-combustion method to be used in combustors for the low-emission energy generation, establishment of fire protection strategies for prevention of the two-phase hybrid mixture explosion, and development of numerical simulation model for simulating the complex combustion systems.

2. Experimental methods

2.1 Experimental apparatus

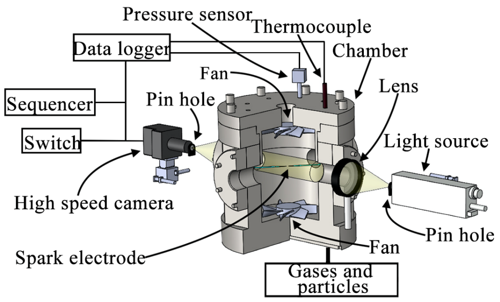

Fig. 1. Schematic of the experimental apparatus.

Fig. 1 depicts the schematic of experimental setup in three-dimensional. The experiments were conducted using a constant-volume spherical chamber measuring 200 mm in diameter and 280 mm in height. The chamber had a total volume of 6.19 × 10 $^{-3}$ m^3. Four quartz glass windows with a diameter of 50 mm were installed to observe the turbulent flame propagation in the chamber. These optical windows were mounted opposite to each other [1,13,21]. To ignite the mixture, a capacitor discharge ignition circuit system was adapted [1,13,21]. The ignition energy was set at 2.8 J, the same as that employed previously for the ignition of ammonia–air and ammonia–methane–air premixtures [13,14]. To facilitate the observation of the combustion, the electrodes were mounted at a 45º angle away from the interrogation path.

Two identical counter-rotation seven-bladed fans were positioned vertically and symmetrically at the top and bottom of the chamber to induce turbulence. Each fan could be accurately rotated between 0 and 15,000 revolutions per minute (rpm) using directly coupled electric motors (Maxon Motor, RE50) with separate speed controllers (Maxon Motor, ESCON 50/5). The fan rotation speed was inaccurate to within ±1 rpm. Particle image velocimetry (PIV) was used to determine the turbulence characteristics (explained in the Appendix—PIV measurement [13,21]). The PIV measurements revealed that, within the observation period, the turbulence was isotropic and homogeneous with almost no evidence of regular bulk motion. Equation (1) was discovered to reflect the turbulence intensity, u', which was proportional to the fan speed, f_s [1,13,21],

$$u' = 0.00129 f_s \quad (1)$$

where f_s denotes the fan speed in rpm. According to two-point correlation, the longitudinal integral length scale, L_f, was 20.9 mm regardless of the turbulence intensity [21]. Besides, the corresponding Reynolds Number under various turbulence intensity used for present research can be seen in Table A in Appendix.

Flame propagation and extinction behavior were observed and recorded by schlieren photography, while the pressure increase inside the chamber during flame propagation was measured with a pressure sensor (Valcom, VPRTF-A4-(−0.1 to 2 MPa) S-5, P1) and recorded by pressure transducer (GRAPHTEC, GL900) at 10 µs intervals. The schlieren photography [1,13], which can capture the position of the high-density gradient caused by the rapid change in gas temperature, detects the preheat zone front. Schlieren photography performed using by a high-speed camera (Phantom, v1212) with an LED light source (Hayashi-repic Co., Ltd., LA-HDF5010C). To create the spotlight effect, a pinhole was fixed in front of the light source The frame rate for the high-speed camera was set as 30000 fps. The camera's resolution was set to 512 pixels × 512 pixels.

2.2 Experimental conditions

To facilitate comparisons, total thermal inputs were kept constant between pure PMMA combustion and PMMA particle cloud–ammonia–air co-combustion. The total thermal heat input from the co-combustion was kept constant with that of the pure PMMA combustion at a particle concentration of 0.3 kg/m^3 by subtracting a portion of the thermal heat input from PMMA particles from the pure ammonia combustion theoretically. The PMMA particle had a lower heating value of 24.4 MJ/kg [22]. The mass of the PMMA particles employed in the co-combustion experiments is shown in Table 1. $\phi_{Ammonia}$ denotes the ammonia–air equivalence ratio in co-combustion. ϕ indicates the ammonia–air equivalence ratio in pure ammonia combustion and silica particle cloud ammonia–air mixing-combustion. Besides, the overall equivalence ratio in co-combustion by considering all PMMA particles being devolatilized can be seen in Table B in Appendix.

Table 1
Calculated PMMA particle mass in co-combustion for maintenance the total thermal heat input is identical to 0.3 kg/m^3 of the PMMA particle concentration

$\phi_{Ammonia}$	PMMA particles needed in the co-combustion field to maintain the total heat input identical to 0.3 kg/m^3 of the PMMA particle concentration [g]
0	1.8570
0.1	1.7594
0.2	1.6670
0.3	1.5794
0.4	1.4961
0.5	1.4170
0.6	1.3417
0.7	1.2699
0.8	1.2013

0.9	1.1359
1.0	1.0733
1.1	1.0134
1.2	0.9560

Notably, the spherical PMMA particles with a diameter of 30 μm employed in this study showed a narrow particle size distribution, which can be considered as the quasi-monodispersed particles

To compare silica particle cloud–ammonia–air mixing combustion with PMMA particle cloud–ammonia–air co-combustion, silica particles with the same mass as PMMA particles were used in the same ammonia equivalence ratio. Furthermore, the ratio of silica particle cloud's heat capacity to heat input in each ammonia equivalence ratio can be seen in Table C in Appendix.

The physical properties of two types of particles can be seen in Table 2 (The micrographs and size distribution data of two types of particles can be observed in Figs. A, B, and C and Tables D, E, F, and G in Appendix).

Table 2 The physical properties of PMMA particle cloud and silica particle cloud

Type of Particle cloud	Particle density [kg/m^3]	Volume mean diameter [m]	Heat capacity [J/kg/K]	Specific surface area [m^2/g]
PMMA	1200	28.813	1466	0.212
Silica	2000	46.8	743	0.31338

Notably, in the current research, mixing combustion is the combustion by mixing nonreactive particles with a gas-fuel–oxidizer mixture. However, co-combustion is the combustion of a hybrid mixture of gas and solid particle fuels.

To clarify the transport behaviors of two types of particles in the near homogeneous turbulent flow field, the Stokes Number [23] was calculated under various turbulence intensities (The detailed values of Stokes number can be seen in Tables H, I, and J in Appendix). The results showed that the particles used for present research are well following the largest scale eddies. However, the particles are not well following the Taylor scale eddies and smallest Kolmogorov scale eddies.

Further, a similar experimental procedure used in our prior studies associated with solid particle cloud–ammonia–oxygen–nitrogen co-combustion [17–19] was used in the co-combustion and mixing combustion experiments presented here. In the first procedure, the particles were equally distributed in four filter cups connected to the inlets. The combustion chamber and the dispersion tank were then emptied to a pressure of 0 kPa using a vacuum pump. Subsequently, the dispersion tank was filled with a mixture of ammonia and air. Similarly, the chamber was supplied with a gas mixture of the same composition. However, the gas mixture in the chamber was set to 75 kPa to ignite the mixture after dispersion at 101 kPa (atmospheric pressure). Within 0.7 s, the dispersion gas swept the particles into the center of the chamber. At the atmosphere pressure, the mixture was ignited 0.3 s after dispersion ended [17,19,20]. Before dispersion, the fans started to rotate for 5 min to achieve the appropriate turbulence intensity. The initial temperature of the mixture for all experiments was constant at 293 ± 3 K. The maximum errors in the concentrations of ammonia or air, pressure, and PMMA particle mass were 1%, 5%, and 3%, respectively. At least three experiments were conducted for each condition to ensure the reliability of the experimental data.

3. Turbulent flame propagation and extinction

Figure 2 shows the turbulent flame propagation and extinction images in PMMA particle cloud–ammonia–air co-combustion at the same ammonia equivalence ratio ($\phi_{Ammonia}$ = 0.4). Supplementary materials provide the video recordings of the schlieren photography associated with Fig. 2 (Video 1: Turbulent flame propagation and Video 2: Turbulent flame extinction). Schlieren photography can capture the particle motion and flame propagation simultaneously during the turbulent flame propagation of the PMMA particle cloud–ammonia–air co-combustion. As shown in Fig. 2, the co-combustion flame can travel outward from the

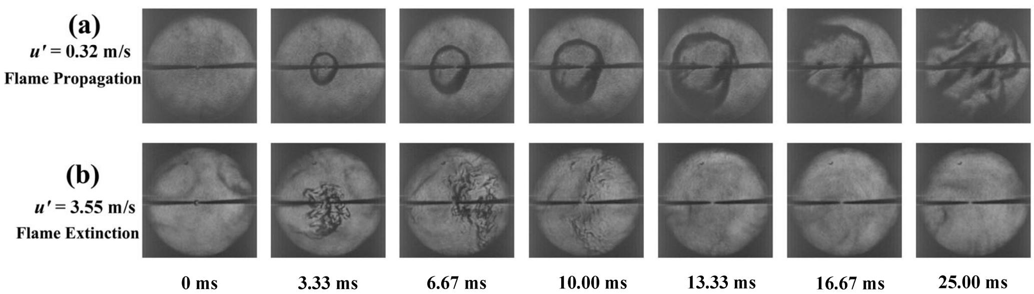

Fig. 2. Turbulent flame propagation and extinction in solid particle cloud–ammonia–air two-phase hybrid mixture co-combustion under $\phi_{Ammonia}$ = 0.4; (a) for flame propagation case; (b) for extinction case.

ignition point to the observation windows edge when u' = 0.32 m/s. However, with u' = 3.55 m/s, the flame propagates first following ignition. Then, when the flame expands, it becomes highly deformed and finally is extinguished by the turbulence. There are numerous small patterns formed in the flame front. This phenomenon is considered to be caused by small-scale eddies in the turbulent flow field deforming the flame. The Kolmogorov and Taylor length scales of the turbulence flow field decrease as the turbulence intensity increases. Consequently, these small-scale eddies act at the flame front to increase the flame surface area. However, when the flame propagated further, the flame was extinguished because of the high flame stretch rate caused by turbulent eddies [24]. For the pure gas combustion, when the characteristic time scale of the chemical reaction is larger than the characteristic time scale of the turbulence disturbance, the chemical reaction cannot be completed at the flame front and eventually the flame is extinguished [13,14]. Although calculating the chemical reaction time scale of the volatile matter–ammonia–air mixture is difficult owing to the complicated combustion process of the solid particles, the difference in characteristic time scales between the chemical reaction of the volatile matter–ammonia–air and the disturbance of the turbulence plays an important role in the turbulent flame extinction of solid particle cloud–ammonia–air co-combustion.

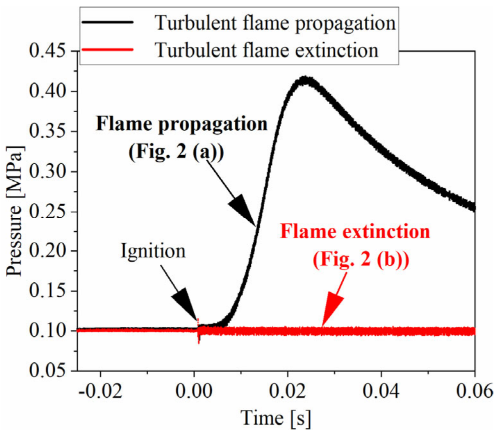

Fig. 3. Pressure history for determining the turbulent flame propagation or extinction in co–combustion.

Each experiment's pressure history was examined to corroborate the turbulent flame propagation and extinction. Figure 3 shows the pressure histories associated with the experimental condition in Fig. 2. As shown in Fig. 3, the pressure inside the camber finally increased in the turbulent flame propagation condition. The combustion reaction increased the pressure in the constant-volume vessel owing to the heat release and temperature rise. However, in the extinction situation, the pressure inside the chamber was almost constant at atmospheric pressure even with the turbulent flame propagation up to its equivalent radius larger than the ignition affected radius. Finally, the pressure history within the chamber during combustion was used to determine the extinction or propagation of the turbulent flame.

4. Results and discussion

4.1 Turbulent flame propagation limits of silica particle cloud–ammonia–air mixing combustion

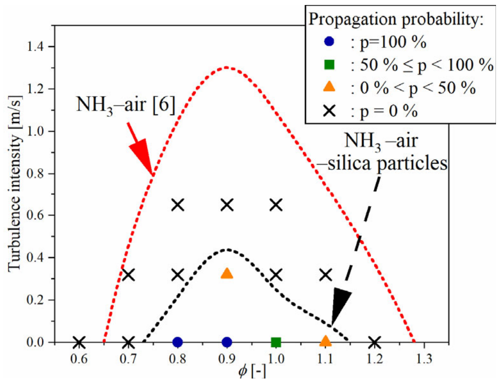

Fig. 4. Turbulent flame propagation map for silica particle cloud–ammonia–air mixing combustion.

Figure 4 shows the turbulent flame propagation probability map for silica particle cloud–ammonia–air flames at the turbulent intensity for various ammonia equivalence ratios. The turbulence intensity at 0 m/s indicates laminar combustion experiments, whereas the other turbulence intensity conditions show turbulent combustion experiments. At least three experiments on turbulent flame extinction were conducted under the same condition, and the same flame propagation or extinction result was not necessarily obtained under the same condition. Additionally, the turbulent flame propagation probabilities, p, were classified into four categories, the blue circle plots representing 100% propagation, green square plots representing 50%–99% propagation, orange triangle plots representing 1%–49% propagation, and black cross-mark plots representing for 0% propagation. The probability was calculated using at least three independent experiments for each condition. The turbulent flame propagation limits were defined between the propagation (p > 0%) and no propagation (p = 0%) plots. A similar method was used to determine the turbulent flame propagation limits for premixed ammonia–air and ammonia–methane–air mixtures [13,14].

As shown in Fig. 4, the black dashed line indicates the turbulent flame propagation limitations of the silica particle cloud–ammonia–air mixture obtained in this work. The red dashed line indicates the turbulent flame propagation limits of the premixed ammonia–

air flame, which were obtained in our previous research [13]. Thus, adding silica particles contracted the turbulent flame propagation limits of the premixed ammonia–air flames. This is considered to be due to the inert silica particle's negative thermal heat sink effect. In the turbulent flame propagation of the silica particle cloud–ammonia–air mixing combustion, the silica particles absorb the heat from the flame. As a result of the addition of the inert silica particles, the flame temperature of the premixed ammonia–air mixture is decreased, and the flame is easily to be extinguished by turbulence eddies.

In pure premixed ammonia–air mixtures, the flame with a 0.9 equivalence ratio can propagate with the highest turbulence intensity despite the fact that the laminar burning velocity achieves a maximum at an equivalence ratio of 1.1. This is caused by the effect of diffusional–thermal instability of the ammonia lean mixture [6]. Even in the silica particle cloud–ammonia–air mixing combustion, the mixture with the same equivalence ratio of 0.9 can propagate at the highest turbulence intensity. Therefore, the diffusional–thermal instability continues to affect the turbulent flame propagation limits of the silica particle cloud–ammonia–air mixture.

Notably, in the turbulent flame propagation of silica particle cloud–ammonia–air mixing combustion, the absorption and desorption of ammonia by silica particles may occur. However, it is considered that the absorption and desorption of ammonia by silica particles have little effect on the final conclusion of the present research. First, the silica particle cloud–ammonia–air mixing combustion experiments were used to clarify the thermal heat sink effect. Second, the detailed flame structure is unchanged between mixing combustion and pure ammonia combustion.

4.2 Turbulent flame propagation limits of PMMA particle cloud–ammonia–air co-combustion

Figure 5 shows the turbulent flame propagation probability map on the turbulence intensity as a function of $\phi_{Ammonia}$ in the PMMA particle cloud–ammonia–air two-phase hybrid-mixture co-combustion. In PMMA particle cloud–ammonia–air co-combustion, the same definition method of the turbulent flame propagation probabilities, *p*, as in the silica particle cloud–ammonia–air mixing combustion was used. As shown in Fig. 5, the black dashed line donates the turbulent flame propagation limits of the silica particle cloud–ammonia–air mixing combustion obtained in Fig. 4. The red dashed line indicates the turbulent flame propagation limits of the premixed ammonia–air combustion [13]. The purple dotted line illustrates the turbulent flame propagation limits of the PMMA particle cloud–ammonia–air co-combustion. Besides, as shown in Fig. 5, $\phi_{Ammonia} = 0$ reflects the turbulent flame propagation limits of pure PMMA particle cloud combustion under a particle concentration of 0.3 kg/m^3. Moreover, in the laminar case (when $u' = 0$ m/s), the flames in PMMA particle–ammonia–air co-combustion can sustain the propagation when $\phi_{Ammonia}$ is ranged from 0.1 to 1.1. However, for pure premixed ammonia–air flames without added reactive particles, the premixtures can only sustain flames when ϕ is between 0.7 and 1.3 [25]. Therefore, adding reactive particles in premixed ammonia–air mixtures can considerably expand the lean flame propagation limits of the premixed

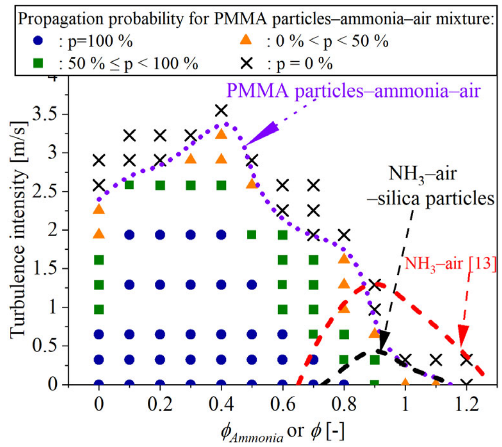

Fig. 5. Turbulent flame propagation probability map for the PMMA particle cloud–ammonia–air co-combustion at the turbulence intensity, u'.

ammonia–air mixture in a laminar condition.

Further, as shown in Fig. 5, when $\phi_{Ammonia}$ is increased from 0 to 1.2, the turbulent flame propagation limits of the premixed ammonia–air mixture were first expanded and then shrunk by adding the PMMA particles. When $\phi_{Ammonia}$ is equal to 0.4, the turbulent flame in PMMA particle cloud–ammonia–air co-combustion can propagate with the highest turbulence intensity. In ammonia lean co-combustion, except for the case with $\phi_{Ammonia} = 0.9$, the inclusion of the PMMA particles expands the turbulent flame propagation limits of the premixed ammonia–air mixture. Conversely, in ammonia stoichiometric and rich conditions, the limits are greatly shrunk by adding the PMMA particles into the mixture. Moreover, the turbulent flame propagation limits of the PMMA particle cloud–ammonia–air co-combustion are the same as those of the silica particle cloud–ammonia–air mixture in ammonia stoichiometric and rich conditions.

There are two types of effects that reactive particles have on the premixed ammonia–air flame during the turbulent flame propagation and extinction of the solid particle cloud–ammonia–air co-combustion. First, as shown in Fig. 4, the inert silica particles absorb heat from the premixed ammonia–air flame to decrease the flame temperature and furtherly shrink the turbulent flame propagation limits of the premixed ammonia–air mixtures. In PMMA particle cloud–ammonia–air co-combustion, not only the sensible heat, but also the heat required for the devolatilization is absorbed by the PMMA particles from the premixed ammonia–air flame. Therefore, the reactive particles function as a heat sink to shrink the turbulent flame propagation limits of the premixed gas-fuel–oxidizer combustion. Second, after the reactive particles being preheated in the preheat zone of the flame front, the particles release the volatile matter, resulting in the local equivalence ratio increment effect [17,18] during co-combustion. The effect of the local equivalence ratio increment on turbulent flame propagation of co-combustion can be positive or negative depending on $\phi_{Ammonia}$. To further clarify the overall effect of PMMA particles on premixed ammonia–air flames, we studied the turbulent flame propagation velocities of PMMA particle cloud–ammonia–air co-combustion and pure premixed ammonia–air combustion at u' = 0.32 m/s.

A same image processing procedure, which was used in our prior studies associated with PMMA particle cloud–ammonia–oxygen–nitrogen co-combustion [18–20], was used in the present research to obtain the turbulent flame propagation velocity. A detailed description of the procedure is described in the Appendix.

Figure 6 shows the turbulent flame propagation velocities of PMMA particle cloud–ammonia–air co-combustion and pure premixed ammonia–air combustion for a range of $\phi_{Ammonia}$ at a constant u' of 0.32 m/s. Further, the turbulent flame propagation velocities of PMMA particle cloud–ammonia–oxygen–nitrogen co-combustion and pure premixed ammonia–oxygen–nitrogen combustion under an oxygen enriched condition (diluted oxidizer: 40% oxygen and 60% nitrogen) at a constant u' of 0.32 m/s were also included in Fig. 6 for the comparison.

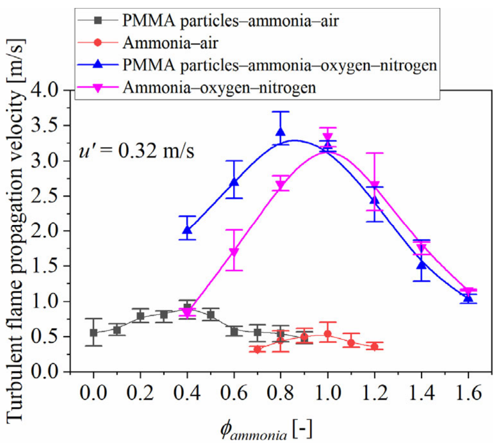

Fig. 6. Turbulent flame propagation velocities of the PMMA particle cloud–ammonia–air co-combustion, PMMA particle cloud–ammonia–oxygen–nitrogen co-combustion, ammonia–air, and ammonia–oxygen–nitrogen premixed flame under u' = 0.32 m/s.

The premixed ammonia–air flame can propagate when ϕ is ranged between 0.7 and 1.2 under u' = 0.32 m/s. However, when $\phi_{Ammonia}$ is ranged from 0.1 to 0.9 in the PMMA particle cloud–ammonia–air mixture, the two-phase hybrid mixture can propagate under the same turbulence intensity. As shown in Fig. 6, when $\phi_{Ammonia}$ is lower than 0.9, the turbulent flame propagation velocity of the PMMA particle cloud–ammonia–air co-combustion is higher than that of the pure premixed ammonia–air flame. When $\phi_{Ammonia}$ is greater than or equal to 0.9 ($\phi_{Ammonia} \geq 0.9$), however, the turbulent flame propagation velocity of co-combustion is lower than that of pure ammonia–air combustion or no flame can maintain in co-combustion. Thus, in PMMA particle cloud–ammonia–air co-combustion, when $\phi_{Ammonia} \leq 0.8$, the local equivalence ratio increment effect has the positive effect of increasing the flame temperature and further increasing the turbulent flame speed. Besides, the positive effect of the local equivalence ratio increment is stronger than the negative effect of the heat sink. Therefore, when $\phi_{Ammonia} \leq 0.8$, the flame temperature of the PMMA particle cloud–ammonia–air co-combustion is higher than that of the pure premixed ammonia–air flame. Finally, the turbulent flame propagation limits of the premixed ammonia–air combustion are expanded by the addition of the PMMA particles. However, when $\phi_{Ammonia} \geq 0.9$, the local equivalence ratio increment effect turns from positive to negative. Consequently, there are two types of negative effects induced by the reactive particles on the flame temperature and flame speed of the premixed ammonia–air flame. Thus, the flame can be quickly doused by adding the PMMA particles when $\phi_{Ammonia} \geq 0.9$.

Besides, as shown in Fig. 5, in PMMA particle cloud–ammonia–air co-combustion with $\phi_{Ammonia} \geq 1$, the turbulent flame propagation limits of the co-combustion are the same as those of the silica particle cloud–ammonia–air mixture. Under $\phi_{Ammonia}$ = 0.9, the local equivalence ratio increment effect and heat sink effect induced by PMMA particles are both considered to induce the negative effect on the turbulent flame propagation and extinction of ammonia–air flame. Furthermore, under $\phi_{Ammonia} > 0.9$ and u' = 0.32 m/s, all flames in PMMA particle cloud–ammonia–air co-combustion are extinguished by turbulent eddies. Therefore, in PMMA particle cloud–ammonia–air co-combustion with $\phi_{Ammonia} \geq 1$, the heat sink effect induced by the unburned particles has a dominant effect to extinguish the premixed ammonia–air flames.

Besides, as shown in Figs. 5 and 6, the PMMA particle cloud–ammonia–air two phase hybrid-mixture for the case with $\phi_{Ammonia}$ = 0.4 can propagate at the highest turbulence intensity where the turbulent flame propagation velocity reaches its maximum. However, for the premixed ammonia–air mixtures, owing to the effect of the diffusional–thermal instability, the mixtures with a 0.9 ammonia equivalence ratio can propagate at the highest turbulence intensity even though the turbulent flame propagation velocity reaches the maximum near stoichiometric conditions [13]. Thus, adding volatile matter weakens the effect of diffusional–thermal instability on the turbulent flame propagation limits of the premixed ammonia–air flame. Consequently, when the turbulence flame propagation velocity reaches the maximum, the PMMA particle cloud–ammonia–air two-phase hybrid mixture can propagate at the highest turbulence intensity.

Additionally, as shown in Fig. 6, in PMMA particle cloud–ammonia–diluted-oxidizer (diluted oxidizer: 40% oxygen and 60% nitrogen) co-combustion at the same particle concentration, the ammonia equivalence ratio to obtain the equal point of the turbulent flame propagation velocity between the co-combustion and pure ammonia combustion is approximately at ammonia stoichiometric condition. However, as shown in Fig. 6, in PMMA particle cloud–ammonia–air co-combustion, the ammonia equivalence ratio to obtain the equal point of the turbulent flame propagation velocity between co-combustion and pure ammonia combustion is at an ammonia-lean case. This is considered to be caused by the difference in the particle residence time in the preheat zone of the flame front. To clearly clarify this point, the PMMA particle devolatilization time scale (t_{pyro}) and ammonia–air chemical reaction time scale (t_a) were calculated. For the calculation of PMMA devolatilization time scale, a simplified theoretical calculation was conducted by assuming that the ammonia–air flame pass through the stable PMMA particle. The particle temperature and mass were calculated by considering the heat convection between particle and surrounding gas and the heat loss due to devolatilization [26,27]. The detailed calculation can be seen in the Appendix.

Fig. 7 shows the t_{pyro}/t_a as a function of the $\phi_{Ammonia}$ in PMMA particle cloud–ammonia–air co-combustion and PMMA particle cloud–ammonia–oxygen–nitrogen co-combustion.

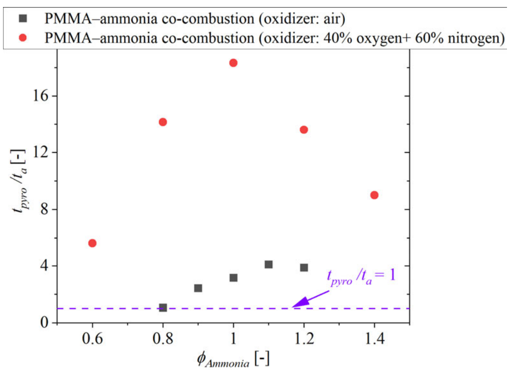

Fig. 7. the t_{pyro}/t_a in PMMA particle cloud–ammonia–air co-combustion and PMMA particle cloud–ammonia–oxygen–nitrogen co-combustion.

As shown in Fig. 7, under a same $\phi_{Ammonia}$, the value of t_{pyro}/t_a in PMMA particle cloud–ammonia–air co-combustion is smaller than that in PMMA particle cloud–ammonia–oxygen–nitrogen co-combustion. Therefore, the particles have ample time to release the volatile matter in the preheat zone of the flame front in PMMA particle cloud–ammonia–air co-combustion. Finally, the effect of the local equivalence ratio increment changes from a positive effect to a negative effect for the case with $\phi_{Ammonia}$ = 0.9. Consequently, in PMMA particle cloud–ammonia–air co-combustion at $\phi_{Ammonia}$ = 0.9, the turbulent flame propagation limit is shrunk by the addition of PMMA particles.

5. Conclusions

In this work, the turbulent flame propagation experiments of silica particle cloud–ammonia–air mixing combustion and polymethylmethacrylate (PMMA) particle cloud–ammonia–air co-combustion were conducted using a fan-stirred constant-volume vessel to determine the effect of particle addition on turbulent flame propagation limits of the premixed ammonia–air mixtures. The principal findings are summarized as follows.

Adding inert silica particles contracted the turbulent flame propagation limits of the premixed ammonia–air mixtures. This is considered to be due to the negative effect of the thermal heat sink caused by the nonreactive silica particles. In this study, the thermal heat sink effect always has a negative role in the turbulent flame propagation of the premixed gas-fuel–oxidizer mixture.

However, with the addition of the reactive particles, with the increase in the ammonia equivalence ratio from lean to rich cases, the turbulent flame propagation limits of the premixed ammonia–air mixture were first expanded and then contracted. The comparison of the turbulent flame propagation velocity between PMMA particle cloud–ammonia–air co-combustion and pure premixed ammonia–air combustion indicates that the turbulent flame propagation and extinction mechanism in solid particle cloud–ammonia–oxidizer co-combustion is dominated by the local equivalence ratio increment effect caused by the addition of the volatile matter released from the particles and the heat sink negative effect induced by the unburned particles in the preheat zone of the flame front. Additionally, the effect of the local equivalence ratio increment can be positive or negative depending on the ammonia equivalence ratio.

Acknowledgements

This work was supported by JSPS KAKENHI Grant Number JP19180646 and 22K20395. The authors would like to thank Prof. Hideaki Kobayashi and Prof. Akihiro Hayakawa for the helpful discussions and kind support for this research.

References

[1] Y. Xia, G. Hashimoto, K. Hadi, N. Hashimoto, A. Hayakawa, H. Kobayashi, O. Fujita, Turbulent burning velocity of ammonia/oxygen/nitrogen premixed flame in O_2-enriched air condition, Fuel 268 (2020) 117383.

[2] L. Wang, M. Xia, H. Wang, K. Huang, C. Qian, C.T. Maravelias, G.A. Ozin, Greening Ammonia toward the Solar Ammonia Refinery, Joule 2 (2018) 1055–1074.

[3] J. Zhang, T. Ito, H. Ishii, S. Ishihara, T. Fujimori, Numerical investigation on ammonia co-firing in a pulverized coal combustion facility: Effect of ammonia co-firing ratio, Fuel 267 (2020) 117166.

[4] S. Ishihara, J. Zhang, T. Ito, Numerical calculation with detailed chemistry of effect of ammonia co-firing on NO emissions in a coal-fired boiler, Fuel 266 (2020) 116924.

[5] M.K. Geikie, K.A. Ahmed, Lagrangian mechanisms of flame extinction for lean turbulent premixed flames, Fuel 194 (2017) 239–256.

[6] A. Hayakawa, Y. Arakawa, R. Mimoto, K.D.K.A. Somarathne, T. Kudo, H. Kobayashi, Experimental investigation of stabilization and emission characteristics of ammonia/air premixed flames in a swirl combustor, Int. J. Hydrogen Energy 42 (2017) 14010–14018.

[7] S. Colson, M. Kuhni, A. Hayakawa, H. Kobayashi, C. Galizzi, D. Escudié, Stabilization mechanisms of an ammonia/methane non-premixed jet flame up to liftoff, Combust. Flame 234 (2021) 111657.

[8] S. Colson, M. Kuhni, C. Galizzi, D. Escudié, H. Kobayashi, Study of the Combined Effect of Ammonia Addition and Air Coflow Velocity on a Non-premixed Methane Jet Flame Stabilization, Combust. Sci. Technol. 00 (2020) 1–21.

[9] A.A. Khateeb, T.F. Guiberti, G. Wang, W.R. Boyette, M. Younes, A. Jamal, W.L. Roberts, Stability limits and NO emissions of premixed swirl ammonia-air flames enriched with hydrogen or methane at elevated pressures, Int. J. Hydrogen Energy 46 (2021) 11969–11981.

[10] E.C. Okafor, H. Yamashita, A. Hayakawa, K.D.K.A. Somarathne, T. Kudo, T. Tsujimura, M. Uchida, S. Ito, H. Kobayashi, Flame stability and emissions characteristics of liquid ammonia spray co-fired with methane in a single stage swirl combustor, Fuel 287 (2021) 119433.

[11] S. Wiseman, M. Rieth, A. Gruber, J.R. Dawson, J.H. Chen, A comparison of the blow-out behavior of turbulent premixed ammonia/hydrogen/nitrogen-air and methane–air flames, Proc. Combust. Inst. 38 (2021) 2869–2876.

[12] C. Lhuillier, P. Brequigny, F. Contino, C. Mounaïm-Rousselle, Experimental investigation on ammonia combustion behavior in a spark-ignition engine by means of laminar and turbulent expanding flames, Proc. Combust. Inst. 38 (2021) 6671–6678.

[13] R. Ichimura, K. Hadi, N. Hashimoto, A. Hayakawa, H. Kobayashi, O. Fujita, Extinction limits of an ammonia/air flame propagating in a turbulent field, Fuel 246 (2019) 178–186.

[14] G. Hashimoto, K. Hadi, Y. Xia, A. Hamid, N. Hashimoto, A. Hayakawa, H. Kobayashi, O. Fujita, Turbulent flame propagation limits of ammonia/methane/air premixed mixture in a constant volume vessel, Proc. Combust. Inst. 38 (2021) 5181–5190.

[15] M. Taniguchi, Flame Propagation Velocity for Co-combustion of Pulverized Coals and Gas Fuels, Energy & Fuels 35 (2021) 6305–6314.

[16] T. Suda, K. Masuko, J. Sato, A. Yamamoto, K. Okazaki, Effect of carbon dioxide on flame propagation of pulverized coal clouds in CO2/O2 combustion, Fuel 86 (2007) 2008–2015.

[17] Y. Xia, K. Hadi, G. Hashimoto, N. Hashimoto, O. Fujita, Effect of ammonia/oxygen/nitrogen equivalence ratio on spherical turbulent flame propagation of pulverized coal/ammonia co-combustion, Proc. Combust. Inst. 38 (2021) 4043–4052.

[18] Y. Xia, N. Hashimoto, O. Fujita, Turbulent flame propagation mechanism of polymethylmethacrylate particle cloud–ammonia co-combustion, Combust. Flame. 241 (2022) 112077.

[19] K. Hadi, R. Ichimura, G. Hashimoto, Y. Xia, N. Hashimoto, O. Fujita, Effect of fuel ratio of coal on the turbulent flame speed of ammonia/coal particle cloud co-combustion at atmospheric pressure, Proc. Combust. Inst. 38 (2021) 4131–4139.

[20] Y. Xia, N. Hashimoto, O. Fujita, Turbulent flame propagation of polymethylmethacrylate particle clouds in an O_2/N_2 atmosphere, Combust. Flame. 234 (2021) 111616.

[21] K. Hadi, R. Ichimura, N. Hashimoto, O. Fujita, Spherical turbulent flame propagation of pulverized coal particle clouds in an O_2/N_2 atmosphere, Proc. Combust. Inst. 37 (2019) 2935–2942.

[22] H.L. Girdhar, G.M. Peerzada, D. Handoo, Specific enthalpies of combustion of some acrylic polymers, Fuel 64 (1985) 1011–1013.

[23] C.T. Crowe, J.D. Schwarzkopf, M. Sommerfeld, Multiphase Flow in Droplets and Particles, CRC press, Boca Raton, 2011.

[24] K.K. Kuo, R. Acharya, Fundamentals of Turbulent and Multiphase Combustion, John Wiley & Sons, Inc., New Jersey, 2012.

[25] H. Kobayashi, A. Hayakawa, K.D.K.A. Somarathne, E.C. Okafor, Science and technology of ammonia combustion, Proc. Combust. Inst. 37 (2019) 109–133.

[26] N. Hashimoto, R. Kurose, S.M. Hwang, H. Tsuji, H. Shirai, A numerical simulation of pulverized coal combustion employing a tabulated-devolatilization-process model (TDP model), Combust. Flame 159 (2012) 353–366.

[27] S. Badzioch, P.G.W. Hawksley, Kinetics of Thermal Decomposition of Pulverized Coal Particles, Ind. Eng. Chem. Process Des. Dev. 9 (1970) 521–530.